This is the Pre-Published Version.

ARTICLE

Acceptor modification of diindolocarbazole embedded multiple-resonance emitters for efficient narrowband deep-blue OLEDs with $CIE_y \leqslant 0.08$ and alleviated efficiency roll-off

Shuxin Wang,[a,b] Jianping Zhou,[c] Jibiao Jin,[a,b] Minqiang Mai,[c] Chui-Shan Tsang,[a] Lawrence Yoon Suk Lee,[a] Lian Duan*[c] and Wai-Yeung Wong*[a,b]

Diindolocarbazole embedded multiple-resonance emitters have shown their unique advantages for narrowband deep-blue organic lighting emitting diodes (OLEDs). However, the severe efficiency roll-off still challenges their further applications. Herein, two efficient narrowband deep-blue emitters, pICz-PPO and pICz-2PPO, were designed and synthesized via acceptor modification strategy to optimize the charge carrier mobility and thus the efficiency roll-off issue was addressed. Both emitters show narrowband deep-blue emission with narrow full width of half maximum (FWHM), high efficiency, and excellent color purity. The pICz-2PPO device exhibits high maximum external quantum efficiency (EQE_{max}) of 17.7% and pure deep-blue emission peaking at 441 nm with a narrow FWHM of 24 nm and CIE coordinate of (0.16, 0.07). More importantly, the significantly alleviated efficiency roll-off is achieved by taking advantages of the balanced charge carrier mobility introduced by the PPO unit with excellent electron-transporting ability, manifesting that the appropriate charge carrier mobility modification can validly suppress efficiency roll-off without the sacrifice of the efficiency and color purity. Surprisingly, pICz-2PPO device exhibits the highest EQE of 12.8% amongst all the reported deep-blue devices based on pICz derivatives (below 10%) at the equivalent brightness of 100 cd m^{-2}. This work provides a guidance to develop efficient multiple-resonance materials for OLEDs with low efficiency roll-off.

Introduction

Achieving high-performance pure deep-blue organic light-emitting diodes (OLEDs) remains a formidable challenge for contemporary ultrahigh-definition (UHD) displays applications.[1] Currently, commercialized displays typically adopt color filters and optical microcavities to compensate for the relatively broad emission of conventional organic emitters, which inevitably suppresses the light extraction, resulting in the depressed external quantum efficiency (EQE).[2–4] Therefore, the development of pure deep-blue emitters with narrowband emission and high efficiency is increasingly prevalent due to their good potentials to reduce power consumption and realize wide color gamut for UHD displays.[5–7] Recently, multiple-resonance (MR) organic emitters have emerged as promising candidates to overcome the drawbacks of conventional OLEDs driven by their efficient narrowband emission character.[8–20] By integrating an opposite resonance effect of electron-donating unit and electron-withdrawing unit in a fused polycyclic framework, the MR effect could be triggered, which minimizes the bonding/antibonding character and suppresses the vibronic coupling between the ground (S_0) and the lowest excited singlet (S_1) states, giving rise to the guaranteed sharpened spectra.

Inspired by the outstanding properties of DABNA-1, the first ultrapure blue MR emitter reported by Hatakeyama in 2016,[21] numerous blue MR materials have been developed in recent years.[22–28] Till now, most of the MR materials are based on the fused polycyclic π-skeleton with mutually ortho-positioned electron-withdrawing boron (B) and electron-donating nitrogen (N) atoms. Such molecular structure can induce the atomically separated frontier molecular orbitals (FMOs), which generally contributes to the small singlet-triplet energy gap (ΔE_{ST}) and high oscillator strength, enabling the efficient narrowband thermally activated delayed fluorescence (TADF) emission.[29] Albeit breakthroughs have been achieved with high maximum external quantum efficiencies (EQE_{max}) of over 30% and narrowband emission with full width at half-maximum (FWHM) as small as 14 nm,[13] B,N-MR emitters still suffer from sophisticated synthesis procedures relying on initial lithiation by alkyllithium to introduce the boron atom with low yields.[30,31] Additionally, B,N-MR emitters usually exhibit emission peaking beyond 460 nm with $CIE_y > 0.1$, which hardly meet the standard deep-blue Commission International de l'Eclariage (CIE)

coordinate of (0.14, 0.08) by the National Television System Commission (NTSC).[7,13,21,32]

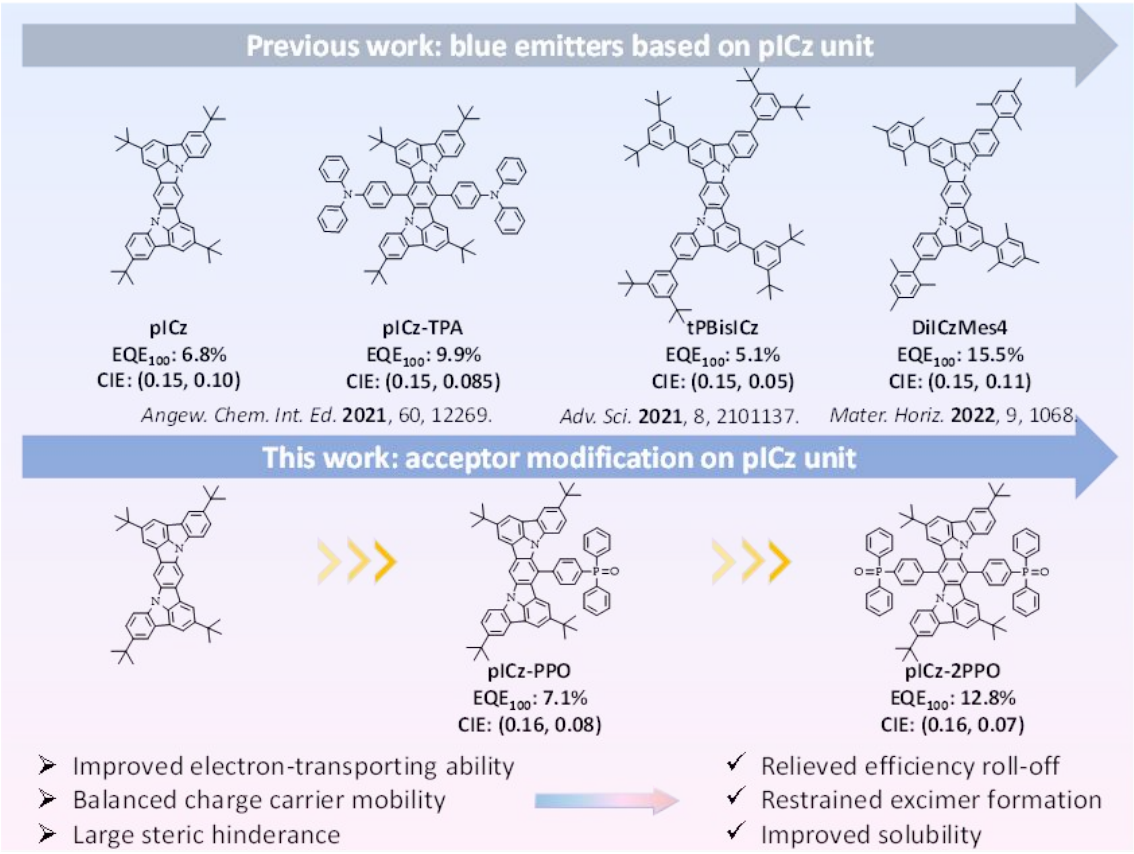

Figure 1. Chemical structures of the reported blue emitters based on pICz units (upper) and the design strategy for pICz-PPO and pICz-2PPO in this work (lower).

Alternatively, Lee et al. demonstrated that the MR effect can also be triggered by different electronegativities of carbon and nitrogen atoms.[33] By fusing two indolo[3,2,1-jk]carbazole (ICz) units with nitrogen atoms at the *meta*-position (mICz), the separation of the highest occupied molecular orbital (HOMO) and the lowest unoccupied molecular orbital (LUMO) on different carbon atoms can be triggered, giving rise to a narrowband violet emission peaking at 393 nm with a small FWHM of 14 nm. Based on this work, several reports successively proposed that further modification of the fusing strategy with nitrogen atoms at the *para*-position (pICz) can shift the emission to the blue region.[34–36] To date, high efficiency with EQE_{max} over 30% has been achieved for this easy-to-be-synthesized blue pICz-based emitters.[34] However, pICz derivatives generally suffer from severe efficiency roll-off (above 70% at 100 cd m^{-2}) and CIE_y > 0.8 (**Figure 1**). Therefore, more investigation on the structural modification for pICz derivatives is of great importance for realizing their potential applications on high-performance pure deep-blue OLEDs.

In this work, a new molecular design strategy towards efficient narrowband deep-blue emitters with alleviated efficiency roll-off was developed. To modify the charge carrier mobility, triphenylphosphine-oxide (PPO) unit with excellent electron-transporting ability is introduced into the pICz core, and thus two narrowband deep-blue emitters pICz-PPO and pICz-2PPO were designed and successfully synthesized. The physical properties were investigated in details through ultraviolet-visible (UV-Vis) absorption and photoluminescence (PL) spectroscopy, theoretical calculations, and thermogravimetric analysis (TGA). The pICz-2PPO devices exhibit not only significantly alleviated efficiency roll-off but also pure deep-blue emission peaking at 441 nm with a narrow FWHM of 24 nm, and CIE coordinate of (0.16, 0.07). Surprisingly, pICz-2PPO device exhibits the highest EQE of 12.8% amongst all the reported deep-blue devices based on pICz derivatives (below 10%) at the equivalent brightness of 100 cd m^{-2}. This work attests to the effectiveness of the charge carrier mobility modification approach in improving the efficiency roll-off without the sacrifice of the color purity for MR emitters.

Results and discussion

Molecular design and synthesis

The efficiency roll-off in OLEDs has been proved to be directly related to the charge carrier mobility of the emitters.[37] Since it is reported that 2-(3-(dibenzo[b,d]thiophen-4-yl)phenyl)indolo [3,2,1-jk]carbazole (ICphth) unit, in which the HOMO and LUMO are mainly distributed over the ICz unit, exhibits a much higher hole mobility ($5.5*10^{-6}$ cm^2/V) than the electron mobility ($2.1*10^{-7}$ cm^2/V),[38] it is reasonable to infer that the charge carrier mobility in pICz is unbalanced with inferior electron-transporting ability. Therefore, in this work, the PPO group with excellent electron-transporting ability[39–42] is introduced to pICz to construct the configurations with more balanced charge carrier mobility, aiming to relieve the efficiency roll-off of the corresponding device. In order to further attest to the effectiveness of PPO unit, two molecules are designed based on pICz moiety with one and two PPOs, respectively, named as pICz-PPO and pICz-2PPO, as shown in **Figure 1**. In addition, the introduction of PPO with peripheral phenyl rings provides sufficient steric hindrance to enable the rigid pICz derivatives with better solubility and suppress the formation of the excimer.

The synthesis procedure is free of reactive alkyllithium reagent with high yields. The pICz-Br was synthesized according to the reported method,[34] and then reacted with diphenyl(4-(4,4,5,5-tetramethyl-1,3,2-dioxaborolan-2-yl)phenyl)phosphine oxide of different stoichiometric proportions to synthesize the targeted products pICz-PPO and pICz-2PPO by the Suzuki-Miyaura coupling reaction. The two emitters were characterized by $^1H/^{13}C$ NMR spectroscopy and mass spectrometry. The thermal properties were investigated by TGA measurements. pICz-PPO and pICz-2PPO exhibit excellent thermal stability with high decomposition temperatures (T_d, corresponding to 5% weight loss) at 514 ℃ and 552 ℃, respectively (**Table 1, Figure S1**). Owing to the large steric hinderance introduced by the PPO group, pICz-PPO and pICz-2PPO exhibit good solubility in common organic solvents such as toluene, dichloromethane, and chloroform. It is noteworthy that pICz-PPO shows better solubility than pICz-2PPO due to its asymmetric structure.

Electrochemical properties and theoretical calculations

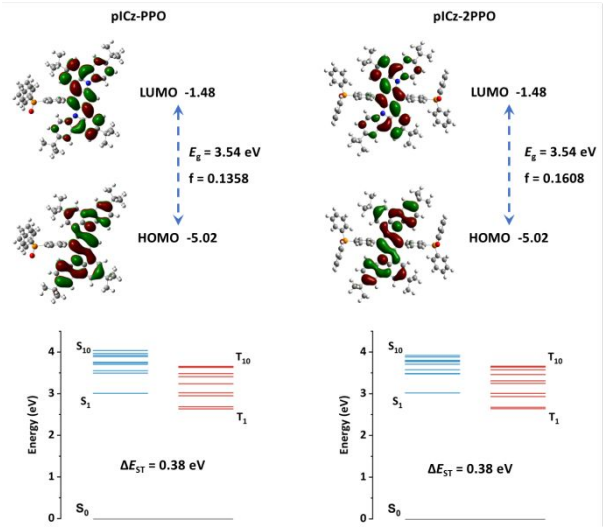

Figure 2. Frontier molecular orbital distribution and energy levels of pICz-PPO and pICz-2PPO.

To investigate the electrochemical properties of the emitters, cyclic voltammetry (CV) measurements were conducted. As shown in **Figure S2**, the oxidation onset against ferrocenium/ferrocene (Fc+/Fc) redox couple for pICz-PPO and pICz-2PPO is 0.95 eV and 0.98 eV, respectively, thus the corresponding HOMO energy is calculated to be -5.34 eV and -5.37 eV. Combined with the bandgap (E_g) energy of 2.8 eV for both pICz-PPO and pICz-2PPO, estimated from the onset of the absorption spectra (**Figure 3a**), the LUMO energy is calculated to be -2.54 eV and -2.57 eV, respectively (**Table 1**).

To gain insight into the geometric and optoelectronic properties, the density functional theory (DFT) and time-dependent DFT (TD-DFT) calculations were conducted using Gaussian program with b3lyp/6-31g(d) basis set. The optimized molecular configurations are shown in **Figure S3**. pICz-PPO and pICz-2PPO exhibit twisted geometry with large dihedral angles of 81-90° between pICz core and peripheral PPO unit, which not only enables their better solubility but also suppresses the formation of the excimer. The calculated frontier molecular

Table 1. Physical properties of pICz-PPO and pICz-2PPO.

Emitters	λ_{em}[a] (nm)	FWHM[b] (nm)	PLQY[c] (%)	Lifetime (ns)	CIE[d] (x, y)	E_g[e] (eV)	HOMO/LUMO[f] (eV)	T_d[g] (℃)
pICz-PPO	438	20	42	7.56	(0.15, 0.03)	2.80	-5.34/-2.54	514
pICz-2PPO	439	19	42	6.02	(0.15, 0.03)	2.80	-5.37/-2.57	552

[a] Emission peak, [b] full width at half maximum, [c] absolute photoluminescence quantum yield, [d] Commission Internationale de l'Eclairage (CIE) coordinates, and [e] optical energy gap measured from the absorption onset in 10^{-5} mol L^{-1} toluene. [f] HOMO calculated from cyclic voltammetry; LUMO derived from HOMO and E_g. [g] Decomposition temperature.

orbital distribution and energy levels of pICz-PPO and pICz-2PPO are shown in **Figure 2**. For both molecules, the atomic localization of HOMO and LUMO was observed over the pICz core with a small fraction extended to the peripheral skeleton, validating its strong MR effect. The singlet-triplet energy gap ΔE_{ST} is calculated to be 0.38 eV, which indicates their non-TADF characters.

Photophysical properties

The UV-Vis absorption, fluorescence (Fl, 300 K) and phosphorescence (Phos, 77K) spectra of pICz-PPO and pICz-2PPO in toluene (10^{-5} mol L^{-1}) are shown in **Figure 3a** and **Figure 3b,** respectively. Two emitters exhibit similar absorption properties, which are also in agreement with the previous reports of pICz-based molecules.[34–36] The absorption bands below 370 nm are assigned to the π-π* transitions of the fused molecular structure,[43] whereas those between 370 nm and 450 nm are attributed to the n-π* transitions of the ICz part.[44] The Fl spectra of pICz-PPO and pICz-2PPO exhibit narrowband deep-blue emission peaking at 438 nm and 439 nm, respectively. Owing to the rigid molecular structure with the MR effect, pICz-PPO and pICz-2PPO show small FWHM of 20 nm and 19 nm, respectively, contributing to their pure deep-blue emission with CIE coordinate of (0.15, 0.03). In addition, small Stokes shifts of pICz-PPO and pICz-2PPO were characterized to be 8 nm and 9 nm, respectively, which indicate the pretty small reorganization energy between the ground and excited states.[45] The Fl spectra of two emitters in doped thin films with dibenzo[b,d]furan-2,8-diylbis(diphenylphosphine oxide) (PPF) as the host were also tested. They show similar emission characters (**Figure 3c**) with their toluene solutions, peaking at 441 nm and 442 nm with FWHM of 21 nm and 20 nm for pICz-PPO and pICz-2PPO, respectively. As shown in **Figure S4**, both emitters exhibit negligible bathochromic shift in different solvents from low-polarity hexane to high-polarity dichloromethane, demonstrating their MR properties.[32] Furthermore, according to the fluorescent and phosphorescent spectra (**Figure 3a, Figure S5**) detected at 77 K, the singlet/triplet energy levels are estimated to be 2.83/2.47 eV for pICz-PPO and 2.82/2.46 eV for pICz-2PPO. The corresponding ΔE_{ST} for both emitters is calculated to be 0.36 eV, which is consistent with the theoretical calculation results. Both emitters exhibit photoluminescence quantum yield (PLQY) of 42% in toluene. The transient PL decay curves were also measured for the two emitters in toluene. As shown in **Figure 3d**, pICz-PPO and pICz-2PPO present mono-exponential profiles with the lifetime of 7.56 ns and 6.02 ns, respectively, and there is no delay component detected. To verify this, the transient PL decay curves were further investigated in doped thin films with PPF as the host. As shown in **Figure S6**, there is only prompt lifetime detected without any delay component, which further manifests their non-TADF characters.

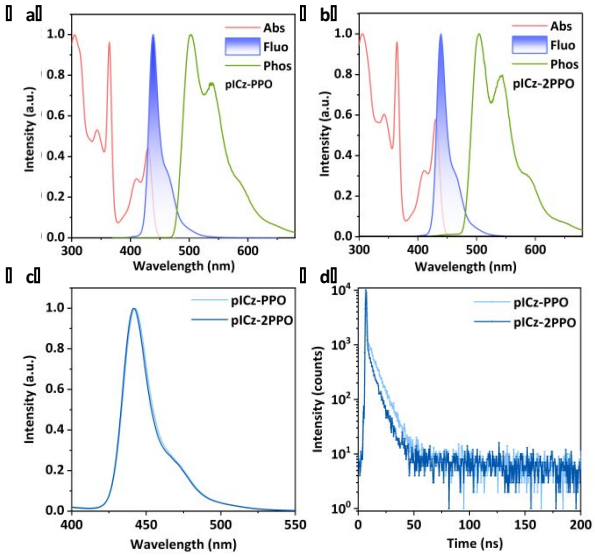

Figure 3. The normalized UV-Vis spectra, fluorescence spectra, phosphorescent spectra (77 K) of (a) pICz-PPO and (b) pICz-2PPO in toluene solution (10^{-5} mol L^{-1}). (c) The normalized fluorescence spectra of doped films of PPF: 1% pICz-PPO and PPF: 1% pICz-2PPO. (d) photoluminescence decay curves of pICz-PPO and pICz-2PPO in toluene solution (10^{-5} mol L^{-1}).

Table 2. Critical parameters for the EL performance of OLEDs with PPF: 30 ωt% m4TCzPhBN: 1 ωt% pICz-PPO / pICz-2PPO as emitting layer.

Device	λ_{EL}[a] (nm)	FWHM (nm)	CIE (x,y)	EQE (%)[b]			V_{on}[c] (V)	PE_{max}[d] ($lm \cdot W^{-1}$)	CE_{max}[e] ($cd \cdot A^{-1}$)
				Max	10 cd m^{-2}	100 cd m^{-2}			
pICz-PPO	442	27	(0.16,0.08)	12.1	10.2	7.1	3.6	8.5	8.7
pICz-2PPO	441	24	(0.16,0.07)	17.7	16.5	12.8	3.6	10.4	12.6

[a] EL emission peak. [b] Maximum external quantum efficiency, and external quantum efficiency at the practical brightness of 10 and 100 cd m^{-2}, respectively. [c] Turn-on voltage at the luminance of 1 cd m^{-2}. [d] Maximum current efficiency. [e] Maximum power efficiency.

Electroluminescence properties

To evaluate the potential application of pICz-PPO and pICz-2PPO for OLEDs, the devices were fabricated to investigate their electroluminescence properties. As shown in **Figure S7a**, the devices were fabricated with the structure of ITO / TAPC (30 nm) / TCTA (5 nm) / mCP (5 nm) / EMLs (20 nm) / PPF (5 nm) / Bphen (30 nm) / LiF (0.5 nm) / Al (150 nm), in which TAPC, TCTA, mCP, PPF and Bphen denote 1,1-bis[4-[N,N'-di(*p*-tolyl)amino]phenyl]cyclohexane, 4,4',4'-tris (carbazol-9-yl)-triphenylamine, 1,3-di-9-carbazolylbenzene, 2,8-bis(diphenylphosphoryl)dibenzo[b,d]furan and 4,7-diphenyl-1,10-phenanthroline, respectively. As for the emitting layer, a binary system was adopted with PPF as the host and pICz-PPO / pICz-2PPO as the emitters (PPF: 1 ωt% pICz-PPO / pICz-2PPO). The EL performances of the fabricated OLEDs are shown in **Figure S7** and **Table S1**. Both devices exhibit narrowband deep-blue emission peaking at 441 nm with a narrow FWHM of 20 nm and CIE coordinate of (0.16, 0.04). However, these two devices suffer from low EQE_{max} with 1.9% and 3.2% for devices based on pICz-PPO and pICz-2PPO, respectively, which indicates that triplet exciton cannot be efficiently harvested through TADF or hot reverse intersystem crossing (RISC) channel.

Given that pICz-PPO and pICz-2PPO can only utilize single excitons for radiative emission, a ternary system for emitting layer was further constructed by employing 2',4',5',6'-tetrakis(3,6-di-*tert*-butyl-9H-carbazol-9-yl)-[1,1':3',1''-terphenyl]-4,4''-dicarbonitrile (m4TCzPhBN) with high reverse intersystem crossing rates and appropriate energy levels[46] as the TADF sensitizer to harvest the triplet excitons and thus enable the devices with efficient exciton utilization (Figure 4a). The PL spectra of PPF: 30 ωt% m4TCzPhBN, PPF: 1 ωt% pICz-PPO / pICz-2PPO, and PPF: 30 ωt% m4TCzPhBN: 1 ωt% pICz-PPO / pICz-2PPO are shown in **Figure S8**. The PL spectra of PPF: 30% m4TCzPhBN: 1% pICz-PPO / pICz-2PPO are nearly identical to that of PPF: 1% pICz-PPO / pICz-2PPO, demonstrating the complete energy transfer from the m4TCzPhBN sensitizer to the pICz-PPO / pICz-2PPO emitters. The transient PL decay curves of PPF: 30% m4TCzPhBN: 1% pICz-PPO / pICz-2PPO are also recorded and shown in **Figure S9**. Different from PPF: 1% pICz-PPO / pICz-2PPO (**Figure S6**), an obvious delay component is detected for PPF: 30% m4TCzPhBN: 1% pICz-PPO / pICz-2PPO, further attesting the efficient sensitizing process described above.

The EL performances of the fabricated OLEDs are shown in **Figure 4**, and some critical parameters are summarized in **Table 2**. Both devices exhibit a low turn-on voltage (3.6 V), indicating the high carrier mobilities of the emitters and the small injection barriers in the devices. The pICz-PPO device exhibits a narrowband deep-blue emission peaking at 442 nm with a narrow FWHM of 27 nm, which is smaller than the FWHM of the previously reported devices based on pICz (41 nm) and pICz-TTA (30 nm) emitters.[34] It can be attributed to its structure with a large steric hinderance introduced by the peripheral PPO unit, which impedes the molecular interactions, leading to the maintained narrowband deep-blue emission. The corresponding CIE coordinate is (0.16, 0.08), which is pretty close to the standard deep-blue CIE coordinate of (0.14, 0.08).

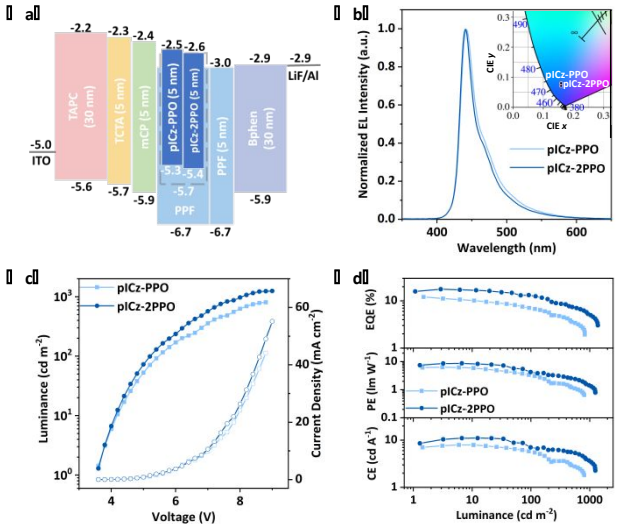

Figure 4. (a) Energy level diagram; (b) electroluminescence spectra (inset shows the corresponding CIE coordinates); (c) luminance-voltage-current density plots and (d) efficiency-luminance characteristics of the OLEDs with PPF: 30 ωt% m4TCzPhBN: 1 ωt% pICz-PPO / pICz-2PPO as emitting layer.

The pICz-PPO device shows the EQE_{max} of 12.1%. Although higher EQE_{max} (> 20%) was observed for the previously reported deep-blue devices with pICz derivatives as emitters at very low brightness, their efficiency roll-off was severe with only 3%-10% EQE at 100 cd m^{-2} (**Table S2**).[34,36] By evaluating the device performance at the equivalent brightness, our pICz-PPO device exhibits comparable overall performance with the previously reported work. Strikingly, the device performance can be dramatically improved through the introduction of another peripheral PPO unit. The pICz-2PPO device exhibits an even better performance with narrower FWHM of 24 nm and higher EQE_{max} of 17.7%. Moreover, it presents greatly suppressed efficiency roll-off with 28% efficiency roll-off at 100 cd m^{-2}, which is significantly alleviated compared to the previously reported deep-blue devices based on pICz derivatives with above 70% efficiency roll-off at the equivalent brightness (**Table S1**). The suppressed efficiency roll-off can be attributed to the more balanced charge carrier mobility of pICz-2PPO introduced by the peripheral PPO unit with excellent electron-transporting ability, indicating that acceptor modification could serve as an effective strategy towards alleviating the efficiency roll-off problem. At the equivalent brightness of 100 cd m^{-2}, pICz-2PPO device is more efficient with higher EQE of 12.8% than that of the previously reported deep-blue devices based on pICz derivatives (below 10%).[34,36]

Conclusions

In summary, a molecular design strategy towards efficient narrowband deep-blue pICz derivatives with alleviated efficiency roll-off was demonstrated by a simple acceptor modification. Through introducing PPO units with excellent electron-transporting ability into the pICz core, two narrowband deep-blue emitters pICz-PPO and pICz-2PPO were successfully designed and synthesized with narrow FWHM, high efficiency, and excellent color purity. The pICz-2PPO device exhibits not only significantly alleviated efficiency roll-off but also high EQE_{max} of 17.7% and pure deep-blue emission peaking at 441 nm with a narrow FWHM of 24 nm, and CIE coordinate of (0.16, 0.07), manifesting that the appropriate modification towards balanced charge carrier mobility contributes to the alleviated efficiency roll-off without the sacrifice of the efficiency and color purity. At the equivalent brightness of 100 cd m^{-2}, pICz-2PPO device exhibits the highest EQE of 12.8% amongst all the reported deep-blue devices based on pICz derivatives (below 10%). Our work attests to fact that modulating the charge carrier mobility is an effective strategy to suppress the efficiency roll-off, paving a new path towards high-performance narrowband deep-blue OLEDs.

Conflicts of interest

There are no conflicts to declare.

Acknowledgements

We acknowledge the National Key R&D Program of China (2022YFE0104100), ITC Guangdong-Hong Kong Technology Cooperation Funding Scheme (TCFS) (GHP/038/19GD), CAS-Croucher Funding Scheme for Joint Laboratories (ZH4A), the Hong Kong Research Grants Council (PolyU 15305320), the Hong Kong Polytechnic University, Miss Clarea Au for the Endowed Professorship in Energy (847S), Research Institute for Smart Energy (CDAQ) and the National Natural Science Foundation of China (22205188) for financial support. L.D. thanks the National Science Fund of China (No. 22135004).

References

1 I. S. Park, M. Yang, H. Shibata, N. Amanokura and T. Yasuda, *Adv. Mater.,* 2022, **34**, 2107951.
2 X. L. Lv, J. S. Miao, M. H. Liu, Q. Peng, C. Zhong, Y. X. Hu, X. S. Cao, H. Wu, Y. Y. Yang, C. J. Zhou, J. Z. Ma, Y. Zou and C. L. Yang, *Angew. Chem. Int. Ed.,* 2022, **61,** e202201588.
3 S. M. Suresh, L. Zhang, T. Matulaitis, D. Hall, C. Si, G. Ricci, A. M. Z. Slawin, S. Warriner, D. Beljonne, Y. Olivier, I. D. W. Samuel and E. Zysman-Colman, *Adv. Mater.,* 2023, **35**, 2300997.
4 X.-C. Fan, K. Wang, Y.-Z. Shi, Y.-C. Cheng, Y.-T. Lee, J. Yu, X.-K. Chen, C. Adachi and X.-H. Zhang, *Nat. Photonics,* 2023, **17**, 280–285.
5 R. Braveenth, H. Lee, J. D. Park, K. J. Yang, S. J. Hwang, K. R. Naveen, R. Lampande and J. H. Kwon, *Adv. Funct. Mater.,* 2021, **31**, 2105805.
6 Y. Y. Gan, X. M. Peng, W. D. Qiu, L. Y. Wang, D. Li, W. T. Xie, D. H. Liu, M. K. Li, J. Y. Lin and S.-J. Su, *Chem. Eng. J.,* 2022, **430**, 133030.
7 H. L. Lee, S. O. Jeon, I. Kim, S. C. Kim, J. Lim, J. Kim, S. Park, J. Chwae, W. Son, H. Choi and J. Y. Lee, *Adv. Mater.,* 2022, **34**, 2202464.
8 X. Luo, S. Song, H. Ni, H. Ma, D. Yang, D. Ma, Y. Zheng and J. Zuo, *Angew. Chem. Int. Ed.,* 2022, **61**, e202209984.
9 Y. Zou, J. H. Hu, M. X. Yu, J. S. Miao, Z. Y. Xie, Y. T. Qiu, X. S. Cao and C. L. Yang, *Adv. Mater.,* 2022, **34**, 2201442.
10 I. S. Park, H. Min and T. Yasuda, *Angew. Chem. Int. Ed.,* 2022, **61**, e202205684.
11 X. Luo, H. Ni, A. Lv, X. Yao, H. Ma and Y. Zheng, *Adv. Opt. Mater.,* 2022, **10**, 2200504.
12 X. Liang, Z.-P. Yan, H.-B. Han, Z.-G. Wu, Y.-X. Zheng, H. Meng, J.-L. Zuo and W. Huang, *Angew. Chem. Int. Ed.,* 2018, **130**, 11486–11490.
13 Y. Kondo, K. Yoshiura, S. Kitera, H. Nishi, S. Oda, H. Gotoh, Y. Sasada, M. Yanai and T. Hatakeyama, *Nat. Photonics,* 2019, **13**, 678–682.
14 S. M. Suresh, E. Duda, D. Hall, Z. Yao, S. Bagnich, A. M. Z. Slawin, H. Bässler, D. Beljonne, M. Buck, Y. Olivier, A. Köhler and E. Zysman-Colman, *J. Am. Chem. Soc.,* 2020, **142**, 6588–6599.
15 H. Tanaka, S. Oda, G. Ricci, H. Gotoh, K. Tabata, R. Kawasumi, D. Beljonne, Y. Olivier and T. Hatakeyama, *Angew. Chem. Int. Ed.,* 2021, **60**, 17910–17914.
16 Y. W. Zhang, D. D. Zhang, J. B. Wei, X. C. Hong, Y. Lu, D. P. Hu, G. M. Li, Z. Y. Liu, Y. Chen and L. Duan, *Angew. Chem. Int. Ed.,* 2020, **132**, 17652–17656.
17 Y. C. Xu, Q. Y. Wang, X. L. Cai, C. L. Li and Y. Wang, *Adv. Mater.,* 2021, **33**, 2100652.
18 Y. W. Zhang, G. M. Li, L. Wang, T. Y. Huang, J. B. Wei, G. Y. Meng, X. Wang, X. Zeng, D. D. Zhang and L. Duan, *Angew. Chem. Int. Ed.,* 2022, **61**, e202202380.
19 M. Yang, I. S. Park and T. Yasuda, *J. Am. Chem. Soc.,* 2020, **142**, 19468–19472.
20 J.-K. Li, X.-Y. Chen, Y.-L. Guo, X.-C. Wang, A. C.-H. Sue, X.-Y. Cao and X.-Y. Wang, *J. Am. Chem. Soc.,* 2021, **143**, 17958–17963.
21 T. Hatakeyama, K. Shiren, K. Nakajima, S. Nomura, S. Nakatsuka, K. Kinoshita, J. Ni, Y. Ono and T. Ikuta, *Adv. Mater.,* 2016, **28**, 2777–2781.
22 K. Matsui, S. Oda, K. Yoshiura, K. Nakajima, N. Yasuda and T. Hatakeyama, *J. Am. Chem. Soc.,* **2018**, *140* (4), 1195–1198.
23 S. Oda, W. Kumano, T. Hama, R. Kawasumi, K. Yoshiura and T. Hatakeyama, *Angew. Chem. Int. Ed.,* 2021, **133**, 2918–2922.
24 P. C. Jiang, J. S. Miao, X. S. Cao, H. Xia, K. Pan, T. Hua, X. L. Lv, Z. Y. Huang, Y. Zou and C. L. Yang, *Adv. Mater.,* 2022, **34**, 2106954.
25 M. Yang, S. Shikita, H. Min, I. S. Park, H. Shibata, N. Amanokura and T. Yasuda, *Angew. Chem. Int. Ed.,* 2021, **60**, 23142–23147.
26 J. K. Bian, S. Chen, L. L. Qiu, R. D. Tian, Y. Man, Y. D. Wang, S. Chen, J. Zhang, C. B. Duan, C. M. Han and H. Xu, *Adv. Mater.,* 2022, **34**, 2110547.
27 J. B. Jin, C. B. Duan, H. Jiang, P. Tao, H. Xu and W.-Y. Wong, *Angew. Chem. Int. Ed.,* 2023, **62**, e202218947.
28 K. R. Naveen, H. Lee, R. Braveenth, K. J. Yang, S. J. Hwang and J. H. Kwon, *Chem. Eng. J.,* 2022, **432**, 134381.
29 X. G. Wu, B. K. Su, D. G. Chen, D. H. Liu, C. C. Wu, Z. X. Huang, T. C. Lin, C. H. Wu, M. B. Zhu, E. Y. Li, W. Y. Hung, W. G. Zhu and P. T. Chou, *Nat. Photonics,* 2021, **15**, 780-786.
30 J. A. Knöller, G. Meng, X. Wang, D. Hall, A. Pershin, D. Beljonne, Y. Olivier, S. Laschat, E. Zysman-Colman and S. Wang, *Angew. Chem. Int. Ed.,* 2020, **59**, 3156–3160.
31 J. A. Knöller, G. Meng, X. Wang, D. Hall, A. Pershin, D. Beljonne, Y. Olivier, S. Laschat, E. Zysman-Colman and S. Wang, *Angew. Chem. Int. Ed.,* 2020, **132**, 3181–3185.

32 T. Hua, J. S. Miao, H. Xia, Z. Y. Huang, X. S. Cao, N. Q. Li and C. L. Yang, *Adv. Funct. Mater.,* 2022, **32**, 2201032.
33 H. L. Lee, W. J. Chung and J. Y. Lee, *Small,* 2020, **16**, 1907569.
34 J. Wei, C. Zhang, D. Zhang, Y. Zhang, Z. Liu, Z. Li, G. Yu and L. Duan, *Angew. Chem. Int. Ed.,* 2021, **60**, 12269–12273.
35 D. Hall, K. Stavrou, E. Duda, A. Danos, S. Bagnich, S. Warriner, A. M. Z. Slawin, D. Beljonne, A. Köhler, A. Monkman, Y. Olivier and E. Zysman-Colman, *Mater. Horiz.,* 2022, **9**, 1068–1080.
36 V. V. Patil, H. L. Lee, I. Kim, K. H. Lee, W. J. Chung, J. Kim, S. Park, H. Choi, W. Son, S. O. Jeon and J. Y. Lee, *Adv. Sci.,* 2021, **8**, 2101137.
37 C. Murawski, K. Leo and M. C. Gather, *Adv. Mater.,* 2013, **25**, 6801–6827.
38 Y. Im, S. H. Han and J. Y. Lee, *Org. Electron.,* 2018, **62**, 560–565.
39 X.-K. Liu, C.-J. Zheng, M.-F. Lo, J. Xiao, C.-S. Lee, M.-K. Fung and X.-H Zhang, *Chem. Commun.,* 2014, **50**, 2027.
40 C. Duan, J. Li, C. Han, D. Ding, H. Yang, Y. Wei and H. Xu, *Chem. Mater.,* 2016, **28**, 5667–5679.
41 C.-H. Chien, C.-K. Chen, F.-M. Hsu, C.-F. Shu, P.-T. Chou and C.-H. Lai, *Adv. Funct. Mater.,* 2009, **19**, 560–566.
42 H. Sasabe, N. Toyota, H. Nakanishi, T. Ishizaka, Y.-J. Pu and J. Kido, *Adv. Mater.,* 2012, **24**, 3212–3217.
43 H. H. Li, Y. Wang, K. Yuan, Y. Tao, R. F. Chen, C. Zheng, X. H. Zhou, J. F. Li and W. Huang, *Chem. Commun.,* 2014, **50**, 15760–15763.
44 P. Kautny, C. Zhao, D. Schopf, B. Stöger, E. Horkel, J. Chen, D. Ma, J. Fröhlich and D. Lumpi, *J. Mater. Chem. C,* 2017, **5**, 1997–2004.
45 X. L. Cai, J. Xue, C. Li, B. Liang, A. Ying, Y. Tan, S. L. Gong and Y. Wang, *Angew. Chem. Int. Ed.,* 2022, **61**, e2022003.
46 D. Zhang, X. Song, A. J. Gillett, B. H. Drummond, S. T. E. Jones, G. Li, H. He, M. Cai, D. Credgington and L. Duan, *Adv. Mater.,* 2020, **32**, 1908355.